Wind Energy

WIND ENERGY
Wind Energ. 2014; **17**:1531–1542
Published online 12 July 2013 in Wiley Online Library (wileyonlinelibrary.com). DOI: 10.1002/we.1649

RESEARCH ARTICLE

Effects of leading edge erosion on wind turbine blade performance

Agrim Sareen, Chinmay A. Sapre and Michael S. Selig

Department of Aerospace Engineering, University of Illinois at Urbana-Champaign, Urbana, IL 61801, USA

ABSTRACT

This paper presents results of a study to investigate the effect of leading edge erosion on the aerodynamic performance of a wind turbine airfoil. The tests were conducted on the DU 96-W-180 wind turbine airfoil at three Reynolds numbers between 1 million and 1.85 million, and angles of attack spanning the nominal low drag range of the airfoil. The airfoil was tested with simulated leading edge erosion by varying both the type and severity of the erosion to investigate the loss in performance due to an eroded leading edge. Tests were also run with simulated bugs on the airfoil to assess the impact of insect accretion on airfoil performance. The objective was to develop a baseline understanding of the aerodynamic effects of varying levels of leading edge erosion and to quantify their relative impact on airfoil performance. Results show that leading edge erosion can produce substantial airfoil performance degradation, yielding a large increase in drag coupled with a significant loss in lift near the upper corner of the drag polar, which is key to maximizing wind turbine energy production. Copyright © 2013 John Wiley & Sons, Ltd.

KEYWORDS

wind turbine; leading edge erosion; performance; aerodynamics

Correspondence

Michael S. Selig, Department of Aerospace Engineering, University of Illinois at Urbana-Champaign, Urbana, IL 61801, USA.
E-mail: m-selig@illinois.edu

Received 25 March 2012; Revised 22 May 2013; Accepted 3 June 2013

1. INTRODUCTION

Wind turbine blades are exposed to precipitation that occurs in a variety of forms and myriad abrasive airborne particles that can, over time, erode their surfaces, particularly at the leading edge. These airborne particles can cause significant blade erosion damage that reduces aerodynamic performance and hence, energy capture. Moreover in some environments, insect debris and other airborne particles can accrete on the leading edges of wind turbine blades. Leading edge blade erosion and debris accretion and contamination can dramatically reduce blade performance particularly in the high-speed rotor tip region that is crucial to optimum blade performance and energy capture.

The erosion process on wind turbine blades typically starts with the formation of small pits near the leading edge, which increase in density with time and combine to form gouges. If left to the forces of nature, the gouges then grow in size and density, and combine to cause delamination near the leading edge. As an example, Figure 1 shows the extent of damage that leading edge erosion can cause on wind turbine blades in service. Figure 1(a) shows a blade with pits and gouges near the leading edge, whereas Figure 1(b) shows a much older blade with delamination over the entire leading edge.

Although the detrimental nature of leading edge erosion is well known across the industry, few efforts have been made to quantify the effect of erosion on wind turbine performance. Previous studies[1–7] have been focused on the accretion of ice, dust, insect debris and leading edge roughness in general on wind turbine blades and not on blade erosion. Additionally, a majority of these studies have been qualitative in nature with not much data presented on the effect of the accretion on wind turbine performance. Nearly all previous studies[8,9] dealing with erosion have used a roughness strip or a zigzag tape applied near the leading edge of the airfoil to simulate surface contamination. Although this approach is widely used because of its simplicity, it does not accurately model leading edge erosion on an actual wind turbine blade, where the shape modification is actually 'negative', that is, eroded away.

The objective of this study was to test a wind turbine airfoil with shape modifications to simulate leading edge erosion going through the evolutionary stages of development. The surface erosion was modeled by observing photographic records

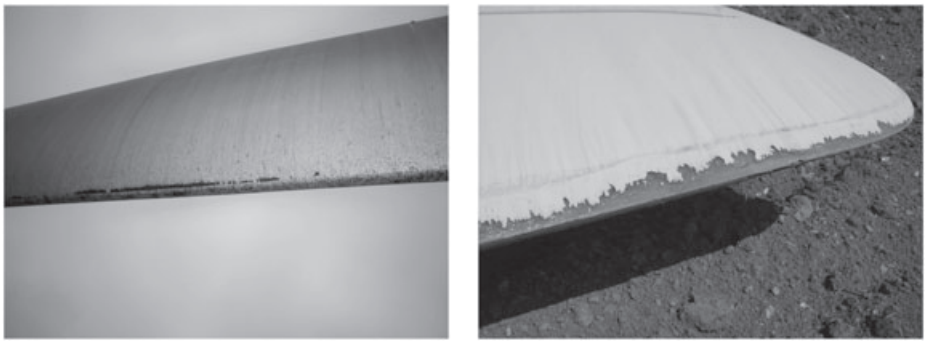

Figure 1. Photographs of wind turbine blades affected by leading edge erosion with (a) pits and gouges, and (b) leading edge delamination (courtesy of 3M).

of wind turbine blades in operation and eroded blades undergoing repair. The goal was to develop a baseline understanding of the aerodynamic effects of various types and magnitudes of leading edge erosion and to quantify their relative impact on airfoil performance. The ultimate aim of conducting the study was to examine the potential detrimental effects of leading edge erosion and consequently, the need for continued development of erosion mitigation strategies.

2. APPROACH AND EXPERIMENTAL METHODS

2.1. Wind tunnel facility

Testing was conducted in the University of Illinois at Urbana-Champaign low-turbulence subsonic wind tunnel shown schematically in Figure 2. The wind tunnel is an open-return type with a 7.5:1 contraction ratio. The rectangular test section is 0.853×1.219 m (2.8×4.0 ft) in cross section and 2.438 m (8 ft) long. Over the length of the test section, the width increases by approximately 1.27 cm (0.5 in) to account for boundary-layer growth along the wind tunnel side walls. Test-section speeds are variable up to 71.53 m/s (160 mph) via a 93.25 kW (125 hp) alternating-current electric motor driving a five-bladed fan. The tunnel settling chamber contains a 10.16 cm (4 in) thick honeycomb and four anti-turbulence screens. The maximum Reynolds number that can be reached is 4.92 million/m (1.5 million/ft).

The airspeed and dynamic pressure in the test section were determined by static pressure measurements in the wind tunnel contraction. Ambient pressure was measured with an absolute pressure transducer. Ambient temperature was measured with a thermocouple. The axial force, normal force and pitching moment of the airfoil were measured using a three-component external force and moment balance mounted underneath the test section. The model was mounted with the spanwise axis in the vertical direction.

Lift and drag were calculated from the normal and axial forces, but a more accurate drag value was determined from wake rake measurements. The rake contained 59 total pressure probes over a total width of 24.77 cm (9.75 in). Seven probes on each of the outer sides of the rake were spaced 6.86 mm (0.27 in) apart, and the remaining inner 45 probes were

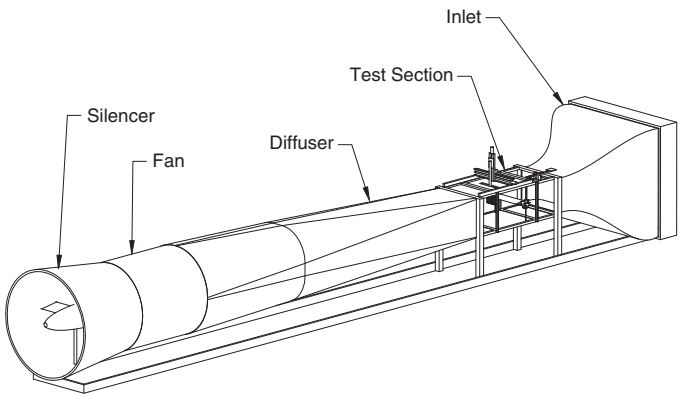

Figure 2. Schematic of the University of Illinois at Urbana-Champaign low-turbulence subsonic wind tunnel.

Wind Energ. 2014; **17**:1531–1542 © 2013 John Wiley & Sons, Ltd.
DOI: 10.1002/we

spaced 3.43 mm (0.135 in) apart. Eight spanwise wake profiles were measured for each angle of attack starting 10.16 cm (4 in) above and ending 7.62 cm (3 in) below center span, and the resulting local drag values were averaged. Only wake rake drag measurements are reported in this paper. All measurements were corrected for wind tunnel effects and validated by comparing data taken for an S809 airfoil model with data taken at Delft and The Ohio State University.[1]

2.2. Erosion models and test plan

The first step in modeling erosion was to understand how erosion develops on wind turbine blades, for which photographs of eroded blades provided by 3M were used. The photographic data set collected by 3M from wind power plant operators covered a range of rotor blade sizes (up to and including megawatt-scale rotors) that had been in operation for 1 year to 10+ years. The photographs revealed that the erosion process starts with the formation of small pits near the leading edge of the blade. As the density of the pits increases with time, they combine to form larger and deeper gouges. This process continues until it ultimately results in delamination centered around the leading edge. The delamination, which starts at the leading edge and grows in its chordwise extent with time, is the final stage of the erosion process. Two important observations were made from the photographs and available literature. Firstly, the density of pits and gouges is maximum near the leading edge and decreases in the chordwise direction. Secondly, there is greater impingement (and therefore greater erosion) on the lower surface because the local average angle of attack is positive for a wind turbine in operation.

Based on the above erosion process, the wind tunnel model was tested with three different types of erosion features: pits, gouges and leading edge delamination. Tests were first run with pits (Type A), then with pits and gouges (Type B) and finally with pits, gouges and leading edge delamination (Type C) to simulate the erosion process. The degree of each type of erosion was also varied in stages, with each successive stage having approximately twice the number of pits and gouges and twice the extent of delamination as the previous one. The size (depth and diameter) and chordwise extent of the pits, gouges and leading edge delamination were based on scaled-down estimates obtained from the photographs of eroded wind turbine blades provided by 3M (Table I). The depth of the pits, gouges and leading edge delamination was set to be 0.51 mm (0.02 in), 2.54 mm (0.10 in) and 3.81 mm (0.15 in), respectively. The average diameter of the pits and gouges was set to be the same as the depth. To account for the differences in the magnitude and chordwise extent of the erosion features on the upper as compared with the lower surface, a ratio of 1:1.3 was used. The ratio was chosen based on observations from the photographic data. Based on this ratio, the chordwise extent of the pits and gouges was fixed for all cases at $s/c \approx 10\%$ on the upper surface and $s/c \approx 13\%$ on the lower surface, and the number of pits and gouges on the lower surface was set to be 1.3 times that on the upper surface. Using the same ratio, the extent of the leading edge delamination was set to $s/c \approx 1\%$, 2% and 3% on the upper surface and $s/c \approx 1.3\%$, 2.6% and 3.9% on the lower surface.

Table II shows the test matrix listing the number of pits and gouges (over the entire model span) and the degree of leading edge delamination on the upper surface of the wind tunnel model for each case (type and stage) tested. As mentioned previously, the number of pits and gouges on the lower surface was 1.3 times those for the upper surface listed in Table II. Moving left-to-right in the table progresses from one type of erosion to the next and moving down along a column progresses from a lower to higher stage (higher degradation). The number of pits (P), number of gouges (G) and extent of delamination (DL) for each case is separated with a slash and listed in the aforementioned order. For example, the Type C/Stage 3 (C3) erosion case had 400 pits and 200 gouges on the upper surface (520 pits and 260 gouges on the lower surface) and light leading edge delamination. Similarly, the Type C/Stage 4 (C4) case had 800 pits and 400 gouges on the upper surface (1040 pits and 520 gouges on the lower surface) and moderate leading edge delamination. Each configuration

Table I. Specifications of the nominal erosion features.

Feature	Depth/Diameter	Leading edge coverage
Pits (*P*)	0.51 mm (0.02 in)	0–50.8 mm (0–2 in)
Gouges (*G*)	2.54 mm (0.10 in)	0–50.8 mm (0–2 in)
Delamination (*DL*)	3.81 mm (0.15 in)	0–4.57/9.14/18.29 mm (0–0.18/0.36/0.72 in)

Table II. Test matrix with the approximate number of pits (*P*), number of gouges (*G*), and magnitude of leading edge delamination (*DL*) on the upper surface of the erosion model for each case tested.

	Type A	Type B	Type C
Stage 1	100*P*	—	—
Stage 2	200*P*	200*P*/100*G*	—
Stage 3	400*P*	400*P*/200*G*	400*P*/200*G*/*DL*
Stage 4	—	800*P*/400*G*	800*P*/400*G*/*DL*+
Stage 5	—	—	1600*P*/800*G*/*DL* + +

(type and stage) was tested at three Reynolds numbers: $Re = 1{,}000{,}000$, 1,500,000 and 1,850,000. All of the cases that were tested were representative of actual observations and based on erosion data and photographs from 3M.

The airfoil used for the tests was the DU 96-W-180. The DU 96-W-180 is an 18% thick airfoil designed at Delft University, Netherlands.[10] It was designed to be used at the 75% blade station. In addition to being used on wind turbines in operation, it is actively used in wind energy research and found in literature.[10–12] To fill the test matrix in Table II, two wind tunnel models were used for the tests. The models had a span of 0.851 m (33.5 in) with a 0.457 m (18 in) chord. Erosion was slowly applied to the models starting with Type A, and moving on to Type B and then Type C. After each model was tested for a particular case, it was returned to the model shop, eroded to the next stage and re-tested. Using the two wind tunnel models, the process continued until all the cases were covered.

The locations of the erosion features on the models were based on a Gaussian distribution with maximum impingement near the leading edge of the airfoil. This distribution was similar to what would be observed on an eroded wind turbine blade. An illustration showing the distribution of the pits, gouges and the extent of the leading edge delamination was generated for each model, which the model maker then used as a reference and mimicked the erosion distribution on the actual airfoil. Figure 3 shows one such exemplar for the C3 erosion model, with the corresponding distribution of erosion features on the upper and lower surfaces over an 80 mm (3.15 in) span from 0–13% s/c. The model maker was given drawings that

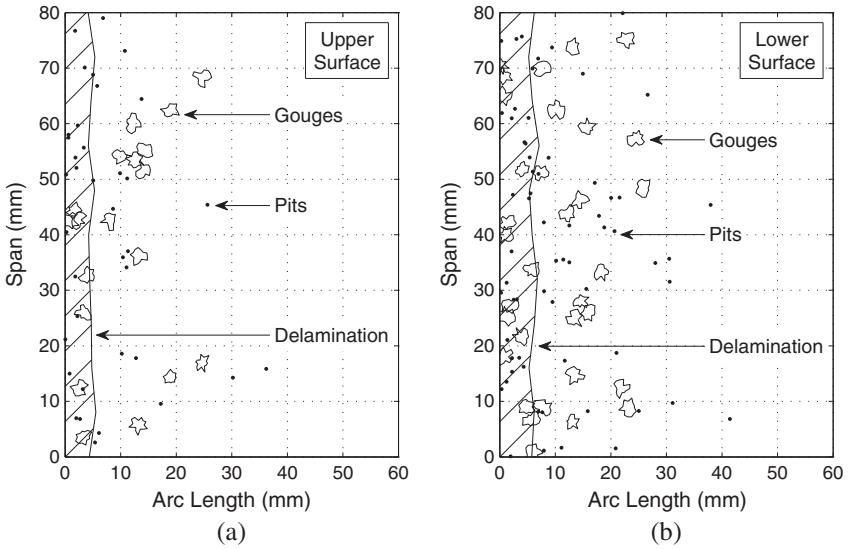

Figure 3. Illustration showing the Type C/Stage 3 (C3) nominal erosion pattern with pits, gouges and leading edge delamination on the (a) upper and (b) lower surface of the DU 96-W-180 erosion model over an 80 mm (3.15 in) span from 0–13% s/c.

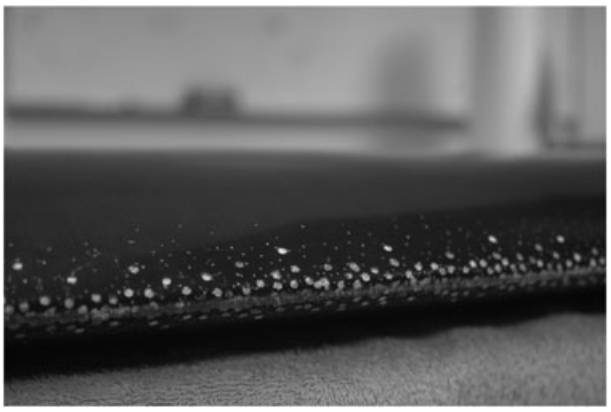

Figure 4. Photograph of the DU 96-W-180 wind tunnel model with Type C/Stage 3 leading edge erosion.

Wind Energ. 2014; **17**:1531–1542 © 2013 John Wiley & Sons, Ltd.
DOI: 10.1002/we

covered the entire span with a unique non-repeating distribution. Figure 4 shows an image of the actual C3 erosion model corresponding to the case shown in Figure 3. Similar photographs were recorded for each erosion model.

In addition to the three types of erosion, the airfoil was also tested with simulated bug strikes by applying a special 0.0035 in (0.09 mm) thick 3M tape cut into small pieces and applied near the leading edge of the wind tunnel model. Simulated bugs were added to the clean airfoil in two stages; the first stage having 35 discrete elements over the entire 33.5 in (0.851 m) span, and the second having 75. Simulated bugs were also added to the model with pits (A1 with 35 bugs and A2 with 75 bugs) to assess the combined effects of both erosion and bugs.

3. RESULTS AND DISCUSSION

This section discusses results of the simulated leading edge erosion and bug tests on the DU 96-W-180 airfoil. Drag polars and lift curves for the different cases along with the percentage increase in drag for each erosion case are shown.

3.1. Clean airfoil

Before testing the DU 96-W-180 airfoil with leading edge erosion, a baseline needed to be determined against which the effect of the leading edge erosion would be compared. Figure 5 shows the performance of the clean DU 96-W-180 airfoil

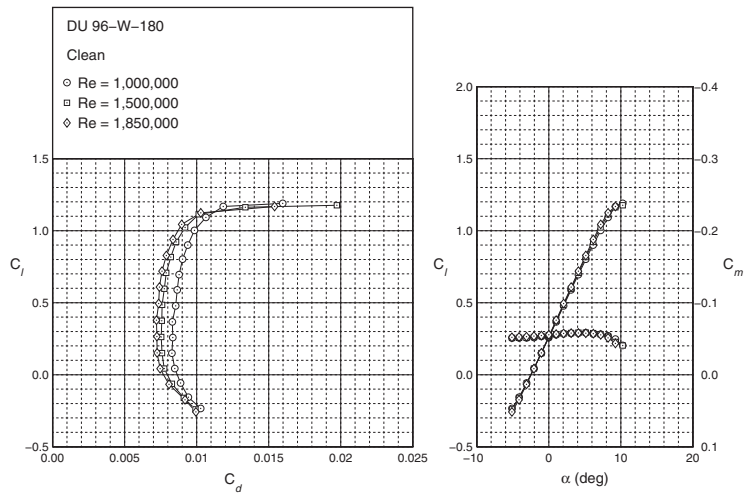

Figure 5. Airfoil characteristics for the clean DU 96-W-180 at the three Reynolds numbers.

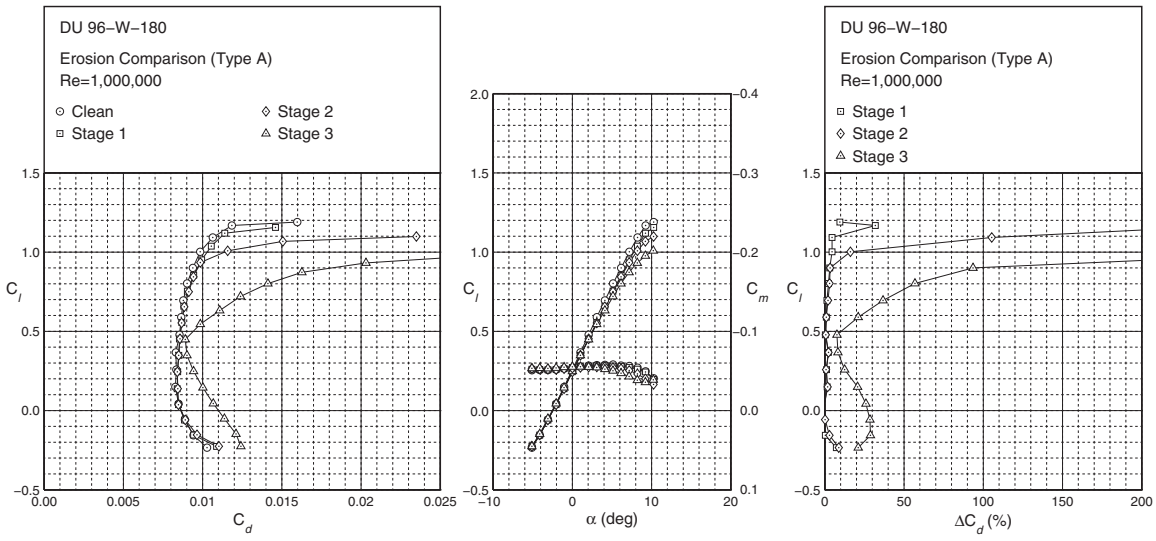

Figure 6. Effect of Type A leading edge erosion on the performance of the DU 96-W-180 airfoil and the resulting percentage increase in drag at $Re = 1{,}000{,}000$.

at the three Reynolds numbers. This data set provided the baseline used to measure the effect of leading edge erosion on the airfoil performance.

3.2. Leading edge erosion

After testing the clean airfoil to obtain the baseline, the erosion models were each tested based on the previously discussed test matrix (Table II). Figures 6–8 show the drag polar, lift curve and quarter-chord pitching moment coefficient for erosion models A1, A2 and A3 compared with the clean airfoil at the three Reynolds numbers. The figures also compare the percentage increase in drag due to leading edge erosion for the three cases. The ΔC_d values were calculated by using the

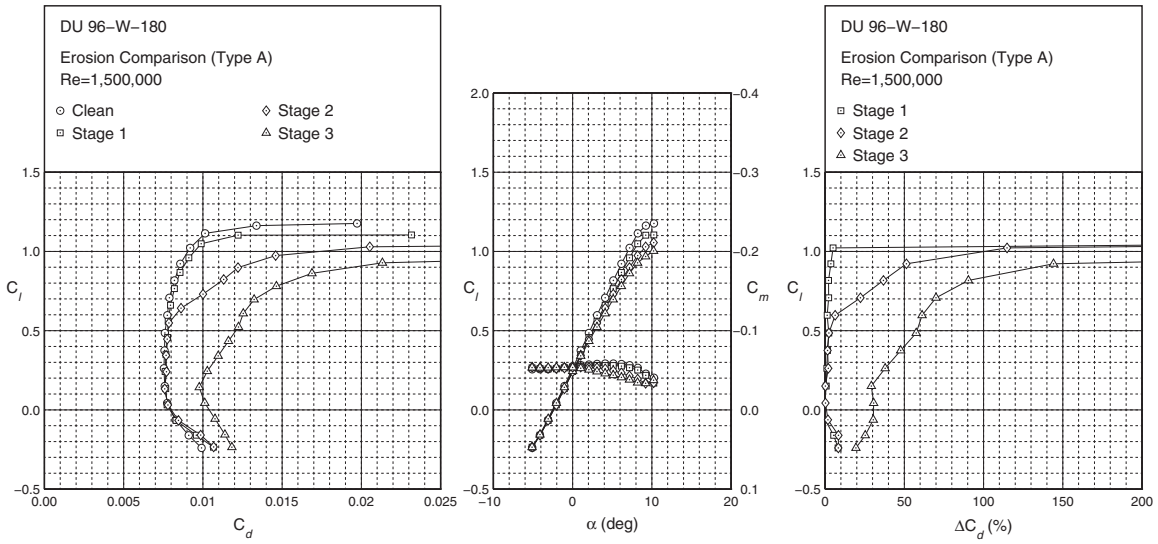

Figure 7. Effect of Type A leading edge erosion on the performance of the DU 96-W-180 airfoil and the resulting percentage increase in drag at $Re = 1{,}500{,}000$.

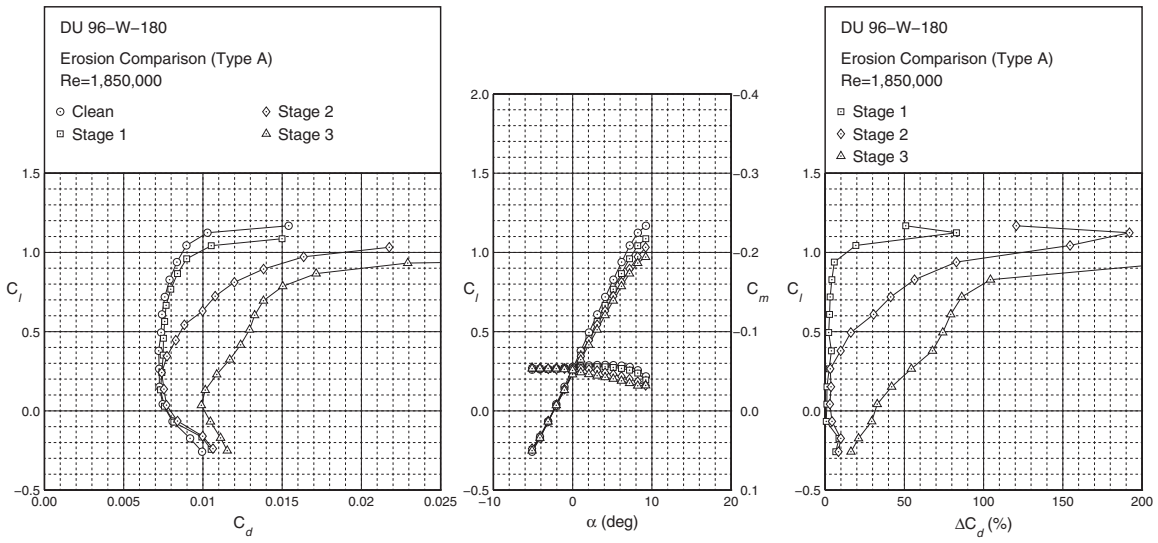

Figure 8. Effect of the Type A leading edge erosion on the performance of the DU 96-W-180 airfoil and the resulting percentage increase in drag at $Re = 1{,}850{,}000$.

Wind Energ. 2014; **17**:1531–1542 © 2013 John Wiley & Sons, Ltd.
DOI: 10.1002/we

clean airfoil as the baseline. The plots show that whereas the first stage of Type A erosion has little impact on the airfoil drag, the detrimental effect of leading edge erosion grows rapidly as the erosion progresses on to Stages 2 and 3. In addition to the increase in drag, the lift curves for these cases also show a significant decrement in lift coefficient at higher angles of attack near $(C_l/C_d)_{\max}$ when clean.

Figures 9–11 and 12–14 show the measurements for erosion cases B2, B3 and B4, and cases C3, C4 and C5, respectively. The plots show similar trends as those for Type A erosion, with the magnitude of degradation in performance increasing progressively as the number of pits, gouges and extent of leading edge delamination increases. The effect of bug strikes on

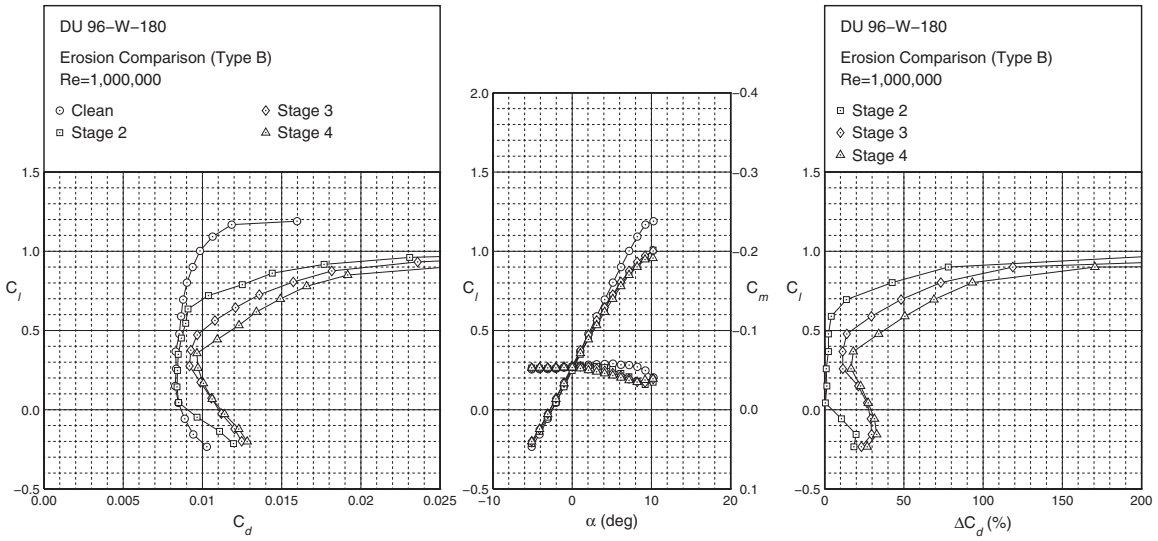

Figure 9. Effect of Type B leading edge erosion on the performance of the DU 96-W-180 airfoil and the resulting percentage increase in drag at $Re = 1{,}000{,}000$.

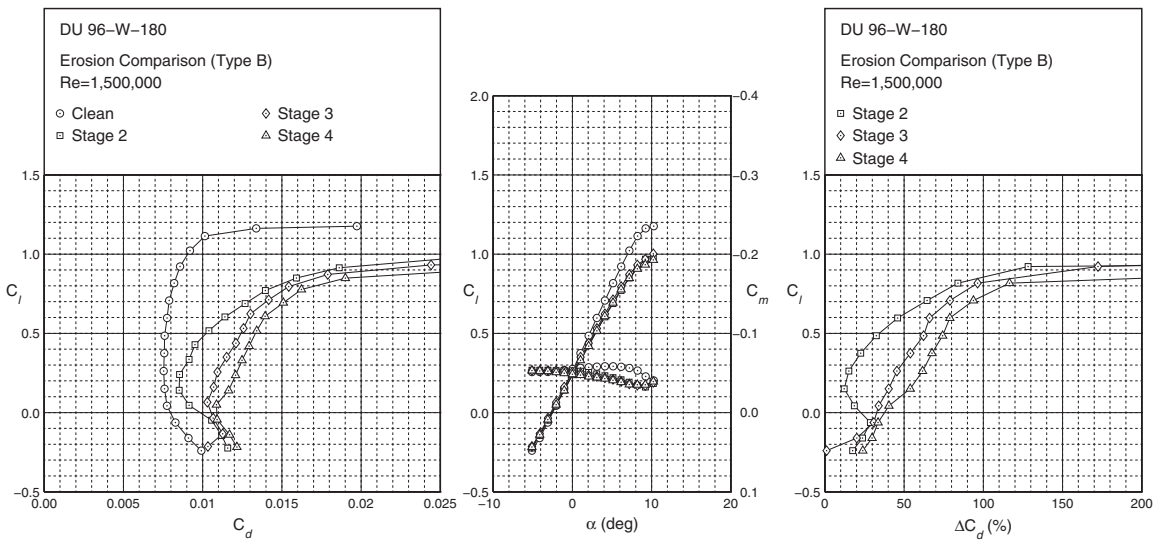

Figure 10. Effect of Type B leading edge erosion on the performance of the DU 96-W-180 airfoil and the resulting percentage increase in drag at $Re = 1{,}500{,}000$.

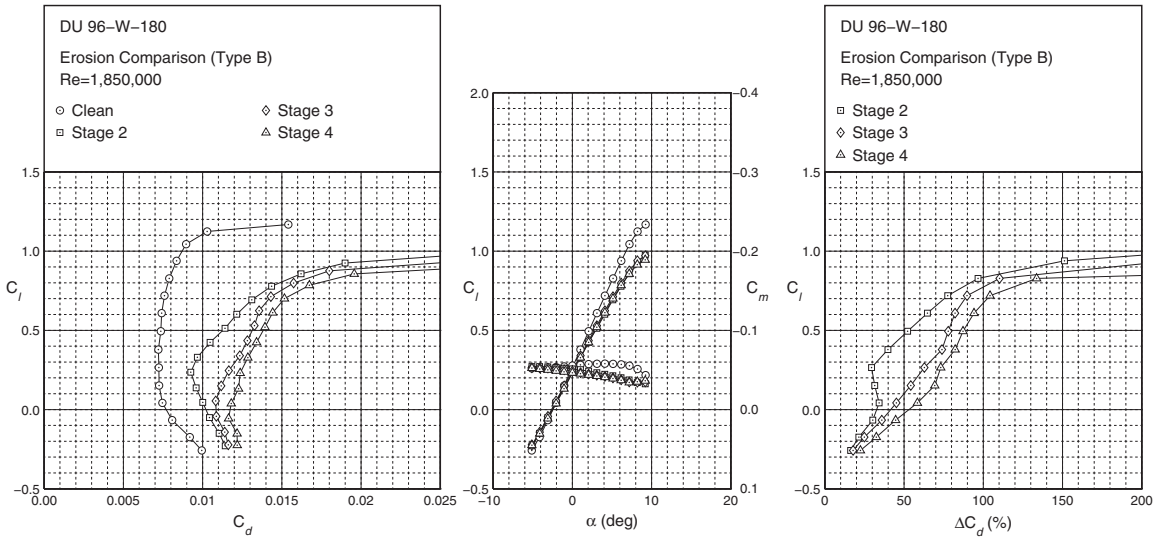

Figure 11. Effect of Type B leading edge erosion on the performance of the DU 96-W-180 airfoil and the resulting percentage increase in drag at $Re = 1{,}850{,}000$.

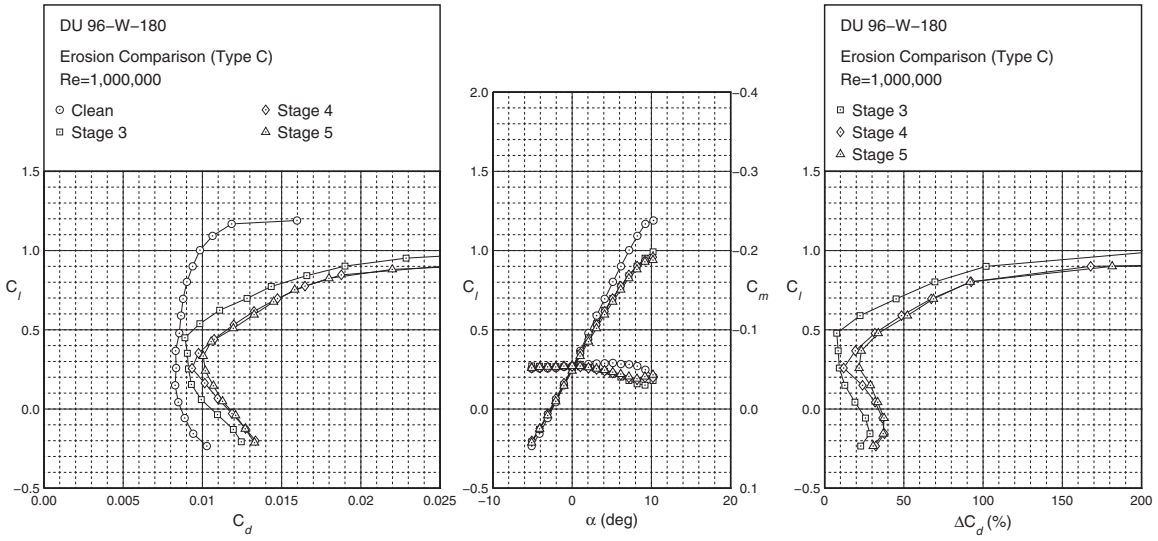

Figure 12. Effect of Type C leading edge erosion on the performance of the DU 96-W-180 airfoil and the resulting percentage increase in drag at $Re = 1{,}000{,}000$.

the airfoil performance can be seen in Figures 15 and 16. Figure 15 shows the drag polar and lift curve for an airfoil with only bugs. Figure 16 shows the combined effects of both bugs and leading edge erosion on the airfoil. The measurements show that bugs can also significantly degrade airfoil performance, both in terms of lift and drag.

3.3. Effects on wind turbine performance

Table III summarizes the detrimental effect of leading edge erosion on the performance of the DU 96-W-180 airfoil. The table lists the percentage increase in drag and the decrement in lift coefficient due to erosion for all cases tested. These losses

Wind Energ. 2014; **17**:1531–1542 © 2013 John Wiley & Sons, Ltd.
DOI: 10.1002/we

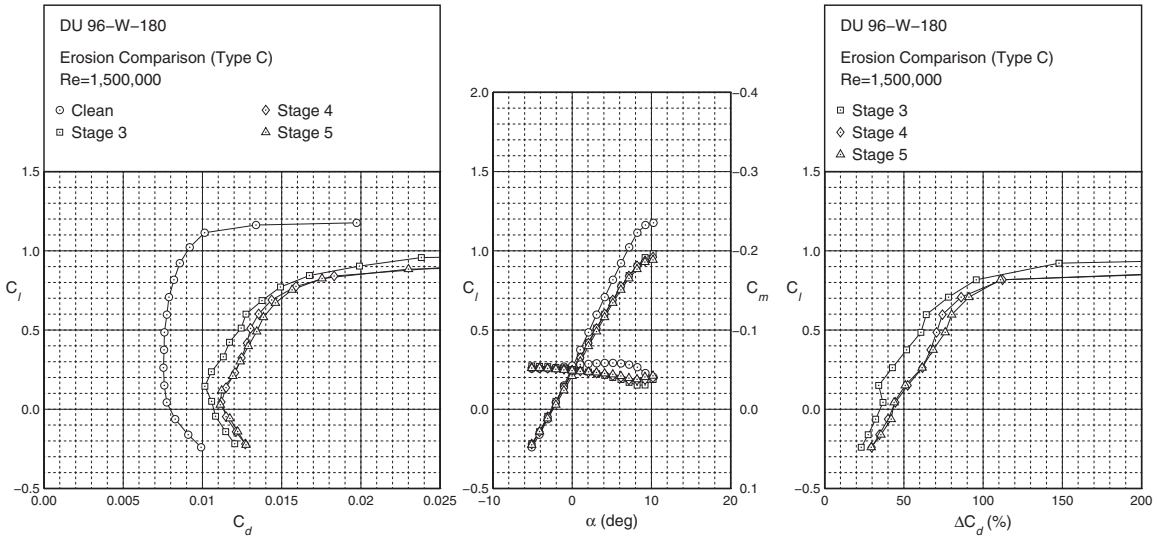

Figure 13. Effect of Type C leading edge erosion on the performance of the DU 96-W-180 airfoil and the resulting percentage increase in drag at $Re = 1{,}500{,}000$.

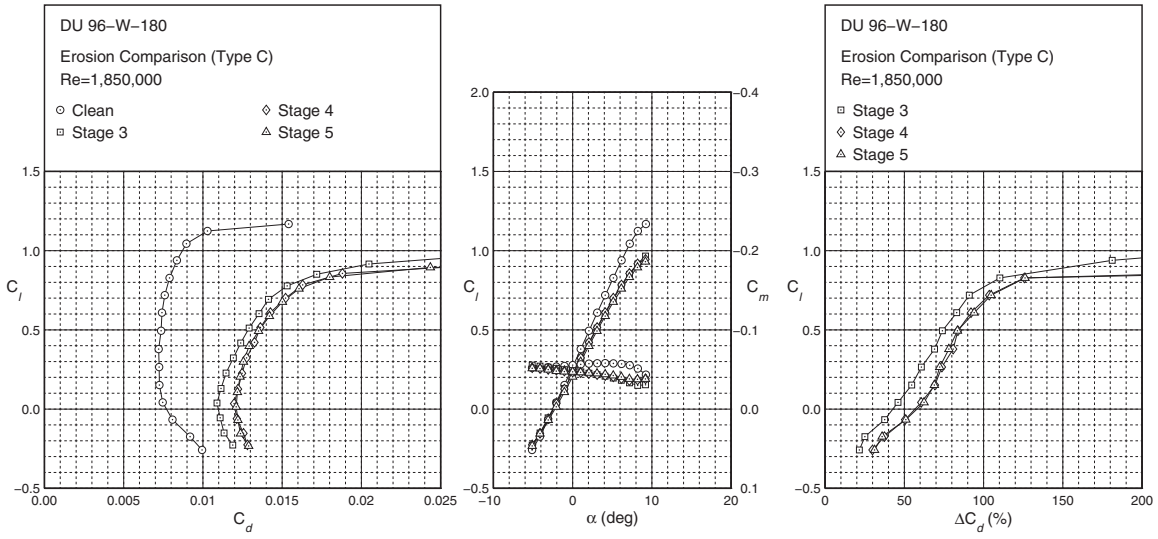

Figure 14. Effect of Type C leading edge erosion on the performance of the DU 96-W-180 airfoil and the resulting percentage increase in drag at $Re = 1{,}850{,}000$.

correspond to a typical variable-speed wind turbine operating condition, that is, near the clean $(C_l/C_d)_{\max}$ operating point. The table also shows the predicted loss in annual energy production (AEP) for erosion models A2, B3 and C4. The data is based on an analysis carried out to estimate the potential loss in performance for a wind turbine with similar leading edge erosion on its blades. The design and analysis was carried out by using the wind turbine design code PROPID.[13] The wind turbine was modeled on a 2.5 MW class turbine and analysed in clean and rough (degraded) conditions to estimate the loss in AEP due to erosion and soiling. Since the Reynolds numbers for a 2.5 MW wind turbine are significantly higher, the analysis was carried out only to estimate the effect on power when assuming the same losses. For all cases, the controller was active in the sense that rotor power reached the rated power of 2.5 MW, albeit at different wind speeds owing to varying

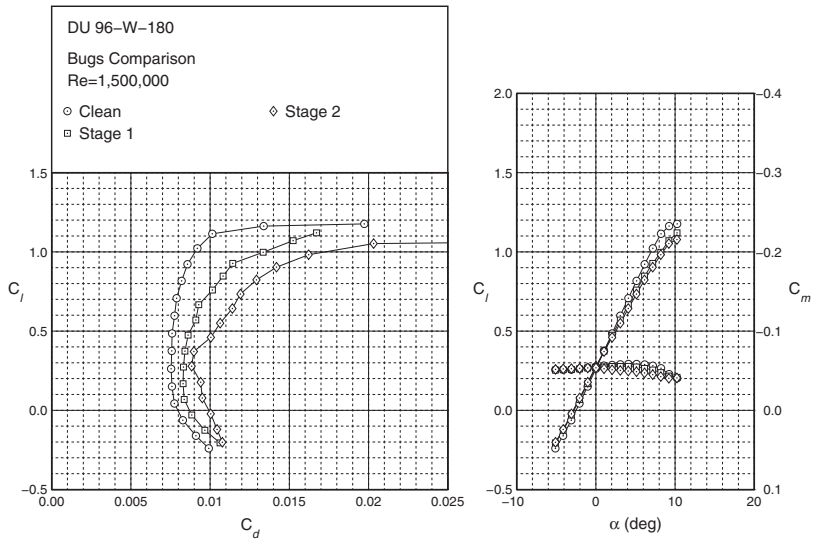

Figure 15. Comparison of the drag polar and lift curve of the clean DU 96-W-180 airfoil and airfoil with bugs at $Re = 1{,}500{,}000$.

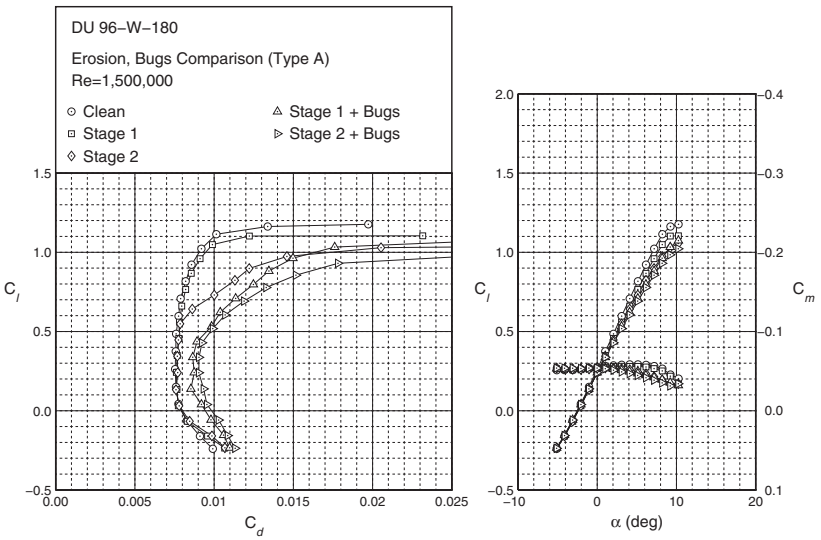

Figure 16. Comparison of the drag polar and lift curve of the clean DU 96-W-180 airfoil and erosion cases A1 and A2 with and without bugs at $Re = 1{,}500{,}000$.

degrees of degradation. The degradation in airfoil performance was applied along the entire blade, but the majority of the AEP loss shown in the the table primarily derives from the outer part of the blade. In the predictions, a Weibull wind speed distribution ($k = 2$) was used.

The tabulated data shows that the measured loss in performance ranges from a 6-500% increase in drag going from light to heavy erosion. The data also shows that the increase in drag is coupled with a significant loss in lift coefficient, which was measured to be as high as 0.17 for the worst case (C5). The AEP loss estimates reveal that even a small amount of leading edge erosion can result in an annual energy loss of approximately 3–5%. The annual energy losses for the heavy erosion cases with pits, gouges and delamination can approach ≈25%, albeit somewhat less in actual application due to a variable distribution of erosion along the blade from hub to tip.

Wind Energ. 2014; **17**:1531–1542 © 2013 John Wiley & Sons, Ltd.
DOI: 10.1002/we

Table III. Effect of leading edge erosion on wind turbine blade performance as estimated by PROPID.

Condition	ΔC_d	ΔC_l	Avg wind speed m/s	AEP loss MWh/yr	AEP loss (%)
A1	+6%	−0.07	—	—	—
			7.05	383	−4.85
A2	+80%	−0.12	7.93	392	−4.10
			8.81	384	−3.49
A3	+150%	−0.15	—	—	—
B2	+150%	−0.16	—	—	—
			7.05	902	−11.42
B3	+200%	−0.14	7.93	930	−9.73
			8.81	917	−8.33
B4	+400%	−0.15	—	—	—
C3	+150%	−0.16	—	—	–
			7.05	1,858	−23.53
C4	+400%	−0.15	7.93	1,948	−20.38
			8.81	1,947	−17.68
C5	+500%	−0.17	—	—	—

4. CONCLUSIONS

The DU 96-W-180 airfoil was tested with various types and magnitudes of leading edge erosion and simulated bug strikes. Results revealed that leading edge erosion can be significantly detrimental to airfoil performance. Data from the tests showed a drag increase of 6–500% due to leading edge erosion (light-to-heavy erosion cases). Erosion also caused a substantial reduction in lift coefficient, especially at the higher angles of attack that are experienced by wind turbines during their operation. Similar to leading edge erosion, simulated bugs on the leading edge also resulted in a significant degradation in airfoil performance. Based on the analysis performed using PROPID, it was estimated that an 80% increase in drag, which was caused by a relatively small degree of leading edge erosion, can result in ≈5% loss in annual energy production. For an increase in drag of 400–500% coupled with the loss in lift, as observed for many of the moderate-to-heavy erosion cases, this loss in annual energy production could be as high as ≈25%. These results shed light on the detrimental effect of leading edge erosion and the need for erosion mitigation strategies. Methods that could reduce or eliminate leading edge erosion would help prevent losses incurred due to the degradation in performance of wind turbine blades after just a few years in operation.

ACKNOWLEDGEMENTS

The authors wish to thank 3M Renewable Energy Division (St Paul, MN) for providing the funding for this research, sample test materials and data on wind turbine erosion and Jennifer L. Kamarainen and her 3M technical team for their cooperation that was instrumental in making this study possible. Also, Performance Composites, Inc. (Compton, CA) is thanked for allowing the inclusion of predictions of performance degradation due to erosion. Finally, the authors thank Shreyas Narsipur for his help with the wind tunnel tests.

REFERENCES

1. Jasinski WJ, Noe SC, Selig MS, Bragg MB. Wind turbine performance under icing conditions. *ASME Journal of Solar Energy Engineering* 1998; **120**: 60–65.
2. Giguère P, Selig MS. Aerodynamic effects of leading-edge tape on airfoils at low Reynolds numbers. *Wind Energy* 1999; **2**: 125–136.
3. van Rooij RPJOM, Timmer WA. Roughness sensitivity considerations for thick rotor blade airfoils. *AIAA Paper 2003–352*, Reno, NV, August 2003.
4. Fuglsang P, Bak C. Development of the Risø wind turbine airfoils. *Wind Energy* 2004; **7**(2): 145–162.

5. Somers DM. The S814 and S815 airfoils, National Renewable Energy Laboratory, NREL/SR-500-36292, December 2004.
6. Khalfallah MG, Koliub AM. Effect of dust on the performance of wind turbines. *Desalination* 2007; **209**(1–3): 209–220.
7. Bak C, Andersen PB, Madsen HA, Gaunaa M. Design and verification of airfoils resistant to surface contamination and turbulence intensity. *AIAA Paper 2008–7050*, Honolulu, HI, August 2008.
8. Giguère P, Selig MS. New airfoils for small horizontal axis wind turbines. *ASME Journal of Solar Energy Engineering* 1998; **120**: 108–114.
9. Solanti MR, Brijandi AH. Effect of surface contamination on the performance of a section of a wind turbine blade. *AIAA Paper 2007-1081*, Reno, NV, January 2007.
10. Timmer WA, van Rooij RPJOM. Summary of the Delft University wind turbine dedicated airfoils. *ASME Journal of Solar Energy Engineering* 2003; **125**: 488–496.
11. Akay B, Ferreira CS, van Bussel GJW, Tescione G. Experimental investigation of the wind turbine blade root flow. *AIAA Paper 2010–641*, Orlando, FL, January 2010.
12. Sareen A, Deters RW, Henry SP, Selig MS. Drag reduction using riblet film applied to airfoils for wind turbines. *AIAA Paper 2011–0558*, Orlando, FL, January 2011.
13. Selig MS, Tangler JL. Development and application of a multipoint inverse design method for horizontal axis wind turbines. *Wind Engineering* 1995; **19**(2): 91–105.

Wind Energ. 2014; **17**:1531–1542 © 2013 John Wiley & Sons, Ltd.
DOI: 10.1002/we